HHS Public Access

Author manuscript

FASEB J. Author manuscript; available in PMC 2024 September 01.

Published in final edited form as:

FASEB J. 2023 September ; 37(9): e23158. doi:10.1096/fj.202300621R.

A Novel Role of RNase L in the Development of Non-Alcoholic Steatohepatitis (NASH)

Guanmin Chen[1], **Xiaotong Zhao**[1], **Maksym Dankovskyy**[1], **Abigail Ansah-Zame**[1], **Uthman Alghamdi**[1], **Danting Liu**[1], **Ruhan Wei**[1], **Jianjun Zhao**[3], **Aimin Zhou**[1,2]

[1]Department of Chemistry, Cleveland State University, Cleveland, OH 44115, USA

[2]Center for Gene Regulation in Health and Diseases, Cleveland State University, Cleveland, OH 44115, USA

[3]Department of Cancer Biology, Cleveland Clinic, Cleveland, OH 44195, USA

Abstract

Nonalcoholic fatty liver disease (NAFLD) is the most common chronic liver disease and affects about 25% of the population globally. NAFLD has the potential to cause significant liver damage in many patients because it can progress to nonalcoholic steatohepatitis (NASH) and cirrhosis, which substantially increases disease morbidity and mortality. Despite the key role of innate immunity in the disease progression, the underlying molecular and pathogenic mechanisms remain to be elucidated. RNase L is a key enzyme in interferon (IFN) action against viral infection and displays pleiotropic biological functions such as control of cell proliferation, apoptosis and autophagy. Recent studies have demonstrated that RNase L is involved in innate immunity. In this study, we revealed that RNase L contributed to the development of NAFLD, which further progressed to NASH in a time-dependent fashion after RNase L wild type (WT) and knockout (KO) mice were fed with a high fat and high cholesterol diet (HFHCD). WT mice showed significantly more severe NASH, evidenced by widespread macro-vesicular steatosis, hepatocyte ballooning degeneration, inflammation, and fibrosis, although physiological and biochemical data indicated that both types of mice developed obesity, hyperglycemia, hypercholesterolemia, dysfunction of the liver, and systemic inflammation at different extents. Further investigation demonstrated that RNase L was responsible for the expression of some key genes in lipid metabolism, inflammation, and fibrosis signaling. Taken together, our results suggest that a novel therapeutic intervention for NAFLD may be developed based on regulating the expression and activity of RNase L.

Graphical Abstract

To whom correspondence should be addressed: Dr. Aimin Zhou, Clinical Chemistry Program, Department of Chemistry, Cleveland State University, Cleveland, OH 44115; Phone: 216-687-2416; Fax: 216-687-9298; a.zhou@csuohio.edu.

Author Contributions: A. Zhou conceived and designed the research; G. Chen, X. Zhao, M. Dankovskyy, A. Ansah-Zame, U. Alghamdi, R. Wei. performed research; D. Liu analyzed the data; G. Chen/A. Zhou wrote the draft; A. Zhou/J. Zhao were involved in reviewing and editing the manuscript. All authors have read and approved the version of the manuscript.

Conflicts of Interest: The authors declare no conflict of interest. The funders had no role in the design of the study; in the collection, analyses, or interpretation of data; in the writing of the manuscript, or in the decision to publish the results.

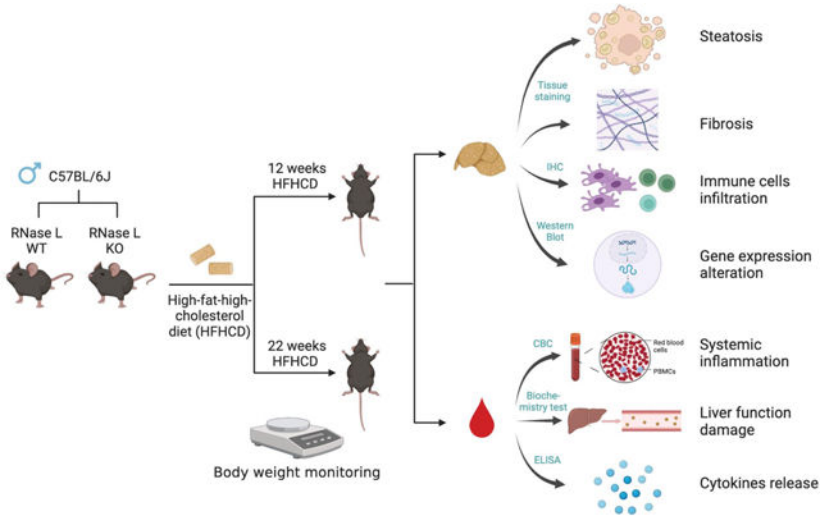

NAFLD is a widespread chronic liver disease, which can progress to NASH and cirrhosis, leading to liver damage. RNase L, a key enzyme in interferon function against viral infection and cell proliferation, contributes to NAFLD progression to NASH. RNase L wild type mice developed more severe NASH than RNase L knockout mice fed with a high fat and high cholesterol diet (HFHCD). Further investigation revealed that RNase L regulates the expression of the key genes in lipid metabolism, inflammation, and fibrosis. (Graphic abstract was created with BioRender.com)

Keywords

RNase L; NAFLD; NASH; High fat high cholesterol diet; Mouse

1. Introduction

Nonalcoholic fatty liver disease (NAFLD), defined as the presence of 5% hepatic steatosis and the absence of secondary causes (e.g., excessive alcohol consumption, medications, or hereditary conditions), has become the leading chronic liver disease over the last decade, currently affecting about 25% of the population worldwide [1]. NAFLD prevalence is expected to increase steadily. In most cases, NAFLD development is closely associated with metabolic risk factors including obesity, dyslipidemia, type 2 diabetes, and hypertension [2]. NAFLD encompasses a spectrum of fatty liver diseases such as nonalcoholic fatty liver (NAFL), nonalcoholic steatohepatitis (NASH) and cirrhosis that indicates the impaired liver function caused by the formation of scar tissue. NASH is defined by steatosis along with hepatocyte damage (hepatocyte ballooning), lobular inflammation, and varying degrees of fibrosis [3]. Persistent NASH could progress to cirrhosis, hepatocellular carcinoma (HCC), and liver failure [4]. It is estimated more than 20% of patients with NASH will develop cirrhosis in their lifetime, which may be the major cause for liver transplants in the US within the next few years [5]. In addition to hepatic complications, NASH patients have a higher risk of developing extrahepatic diseases, for example cardiovascular disease and diabetes [6]. Despite its health threat and economic burden in the society, there is currently no effective therapy for NASH.

Innate immunity is a major contributor to NAFLD progression, in which macrophages are found as the primary mediators of inflammatory response in NASH. Besides, macrophages can promote or attenuate NASH fibrosis based on their polarization status between proinflammatory and reparative phenotypes [7]. Macrophage specific biomarkers and pharmacological agents show promise for the diagnosis and treatment of inflammation and fibrosis in NASH [8]. In NAFLD, macrophages are mainly activated by lipids and lipid metabolites, gut-derived endotoxins, and hepatocellular damage-associated molecules [7]. Lipid accumulation within the liver promotes the formation of certain lipotoxic species that results in cellular toxicity (ER stress and hepatocellular injury), a process termed as "lipotoxicity" that is proposed to be the central pathogenesis of NASH [9,10]. Importantly, lipotoxicity promotes inflammation and the fibrosis process, as these lipotoxic molecules could act on Kupfer Cells (KCs), liver residency microphages, and stellate cells, that are responsible for hepatic fibrosis and activation of the cell signal transduction pathways [10]. Cholesterol is a potential lipotoxic molecule and the addition of excessive cholesterol to a high-fat diet in mouse models causes increased disease severity of NASH [11,12]. Low-density lipoproteins (LDL) are taken in by KCs through the LDL receptor (LDLR), while oxidized low-density lipoprotein (oxLDL) can be taken in by the scavenger receptors (CD36 and SR-A) on the cells, resulting in lysosomal cholesterol accumulation and triggering inflammatory response [13]. Recent studies suggest that exposure of KCs to a high level of cholesterol causes activation of the NLRP3 inflammasome, leading to the production of proinflammatory cytokines and pyroptosis of hepatocytes [14]. Regarding cholesterol-induced NASH, the specific molecular mechanisms involved in cholesterol metabolism, production of proinflammatory genes and activation of the signaling pathways remain to be elucidated.

Ribonuclease L (RNase L) is an interferon (IFN)-inducible enzyme, classically functioning in the 2'-5' linked oligoadenylates (2-5A)/RNase L system of IFN against viral infection and cell proliferation [15]. Upon activation by 2-5A, RNase L cleaves both viral and host RNAs, inducing cell apoptosis and blocking viral replication [16,17]; the small RNA fragments produced by cleavage of target RNAs also initiate signaling events that enhance the production of IFN, promoting innate immune responses [18]. It has been reported that RNase L in immune cells activates the NLRP3 inflammasome during viral infection, subsequently triggering self-cleavage of procaspase-1 and producing IL-1β [19]. Tissue distribution analysis revealed that RNase L is highly expressed in the spleen, thymus and immune cells such as macrophages, suggesting a role of RNase L in the immune system [20]. In our previous study, we have demonstrated that RNase L mediates macrophage function through regulating the expression of pro- and anti-inflammatory genes, such as IL-1β, IL-10, TGF-β, CCL2, and Cox-2 after stimulation with lipopolysaccharides (LPS) [21]. Furthermore, we have recently found that RNase L mediates LPS-induced immune responses independent of its nuclease activity, and RNase L deficiency attenuates the TLR4 signaling pathway [22]. Studies have unraveled that RNase L plays an important role in various human diseases such as cancer [23], cardiac injury [24], acute lung injury [22] and diabetes [20] because of its functions in apoptosis, regulation of proinflammatory gene expression and immune responses. Previously, we have also reported that RNase L functions as an essential regulator of adipogenesis and controls terminal adipocyte differentiation and

lipid storage, suggesting that RNase L is involved in lipid metabolism-associated diseases [25].

In this study, we fed RNase L WT and KO mice with a high fat and high cholesterol diet (HFHCD) for different times and investigated the role of RNase L in the development of NAFLD. We monitored the body weight gain, analyzed the biochemical parameters and immune factors, performed complete blood count (CBC) and evaluated the histological alternations in the livers. The results show that RNase L WT mice exhibited significantly more severe NASH through regulating the expression of some key genes in lipid metabolism, inflammation, and fibrosis signaling, suggesting that RNase L may be a novel target for the design of therapeutic approaches to treat NAFLD.

2. Materials and Methods

2.1. Animal Treatment

Age-matched (9 and 11-months-old) male RNase L WT and KO mice (n = 8/each group) in the C57BL/6 background were fed with a High-Fat-High-Cholesterol Diet (HFHCD) (Envigo, TD160279, Protein 17.3%, carbohydrate 46.7%, Fat 21.2%, cholesterol 2%) either for 12 weeks (9, 11-months-old mice) or 22 weeks (9-months-old mice) to induce NAFLD and NASH. The mice were weighed every week. After the termination of the experiments, the mice were euthanized by CO_2 inhalation and the blood was collected by a heart puncture. Then, a cardiac lavage with PBS (10 ml) was used to remove the remained blood in the tissues. The livers were dissected, and the right lateral lobes of liver tissues were cut and fixed in 10% neutral buffered formalin for at least 48 hours before histological analysis; the rest of the liver tissues were put on dry ice immediately and stored at −80°C for analysis later. This study was carried out in strict accordance with the recommendations in the Guide for the Care and Use of Laboratory Animals of the National Institutes of Health. The protocol (21149-ZHO-AS) was approved on January 4th, 2021, by the Institutional Animal Care and Use Committee (IACUC) of Cleveland State University.

2.2. Mouse Liver Histology and immunohistostaining Analyses

After fixed in the 10% neutral buffered formalin for at least 48 hours, liver tissues with the same location and size were excised and subjected to gradient dehydration and paraffin embedding. The prepared wax blocks were mounted on a microtome and sectioned at 5μm thickness. The slices were affixed to the microscope slides and dried, then deparaffinized through two changes of xylene, followed by rehydration and staining with Hematoxylin & Eosin or Masson's Trichrome staining (Cat#: ab245880 and ab150686, Abcam, Waltham, MA, USA) using standard methods. The stained liver sections were microscopically examined for infiltration of immune cells and morphological alternations. For immunohistostaining, the tissue sections were deparaffinized and rehydrated prior to heat-reduced antigen retrieval in a Barton Pressure Cooker with Sodium Citrate buffer containing 10mM Sodium Citrate, 0.05% Tween 20, pH 6.0 exactly according to the literature method (www.abcam.com/technical). Subsequently, slides were blocked in the blocking solution containing 1 x TBST with 5% Normal Goat Serum (Cat#: #5425, Cell Signaling, Danvers, MA, USA) for one hour, and incubated with rabbit monoclonal

antibodies with a dilution of 1/200 against CD4, CD8, and F4/80 (Cat#: 25229S for CD4; 98941S for CD8 and 70076S for F4/80, Cell Signaling) respectively, followed by incubation with the SignalStain® Boost IHC Detection Reagent that contains a specific HRP-conjugated antibody for rabbit IgG (Cat#: 8114S, Cell Signaling). Color reaction was obtained by subsequent incubation with a diaminobenzidine (DAB) chromogen substrate (SignalStain® DAB Substrate Kit; Cat#:8059S, Cell Signaling). The images were examined with the magnifications at 10 x and 20 x under a Revolve microscope (ECHO, San Diego, CA, USA) at the Center for Gene Regulation in Health and Diseases (GRHD), Cleveland State University.

2.3. Liver Biochemistry Analysis

The whole blood from mice was drawn by a heart puncture using 23-gauge or larger size needles and centrifuged at 1,000 g for 10 minutes at 4°C, and the top plasma layer was collected without disturbing the buffy coat for liver biochemical tests, which were done within 2 hours. The levels of glucose, total cholesterol, triglyceride, alanine transaminase (ALT), and aspartate transaminase (AST) in plasma were analyzed using commercially available slides (Dri-Chem Slides, Heska, Loveland, CO, USA) by a Veterinary Chemistry Analyzer (Element DC5X, Heska) at GRHD.

2.4. Complete Blood Count (CBC)

The whole blood collected from mice was transferred into a purple-top collection tube containing the K salt of ethylenediaminetetraacetic acid (EDTA). The complete blood count was analyzed by the veterinary hematology analyzer (Element HT5, Heska) at GRHD.

2.5. Western Blot Analysis

The liver tissues were homogenized in the ice-cold Triton X-100 lysis buffer containing 50mM Tris-HCl (pH 7.5), 150mM NaCl, 20mM NaF, 1% Triton X-100, 10mM β-glycerol phosphate, 10mM Vanadate and 1 μM protease inhibitors (Cat#:539131, Millipore Sigma, Burlington, MA, USA) by using a tissue grind pestle, followed by sonication with a Branson Digital Sonifier at 0.5 Pulse on/off for 3 seconds on ice. The homogenates were centrifuged at 14,000 g for 20 minutes at 4°C. After centrifugation, the tissue extracts (100 μg per sample) were fractionated on 10% SDS-polyacrylamide gels and transferred to PVDF membranes (Millipore, Billerica, MA, USA). The membranes were blocked with 5% nonfat milk in Tris-buffered saline with 0.2% (v/v) Tween- 20 (TBST), and incubated with different primary antibodies overnight at 4°C. These primary antibodies for NLRP3, Caspase-1, HMGCR, Notch-2, COL1A1 and α-SMA were purchased from Cell Signaling; and for MMP9 and GAPDH were from Abcam and Santa Cruz (Dallas, TX, USA). The membranes were then washed with TBST for 10 min/ 3 times and incubated with specific HRP-linked secondary antibodies (Cell Signaling) for 1 hour at room temperature. After washing, the proteins were detected by a chemiluminescent reagent (Cat#: PI80196, Pierce, Rockford, IL, USA) according to the manufacturer's specification.

2.6. Enzyme-Linked Immunosorbent Assay (ELISA)

IL-1β, CCL2, TNF-α, TGF-β and IL-10 in the plasma and liver tissue extracts were measured by ELISA with commercially available kits (Invitrogen and Thermo Fisher Scientific, Waltham, MA, USA). According to the manufacturer's instruction, flat bottom 96-well ELISA plates were incubated with a capture antibody overnight at 4°C. After incubation, the plates were washed and incubated with the blocking buffer provided with the kit at room temperature (RT) for 1 hour, and then incubated with protein standards and samples overnight at 4°C. After washing, the specific biotin-conjugated detection antibody was added to each well and incubated at RT for 1 hour, followed by washing and incubating with avidin-HRP for 30 minutes. Then, substrates containing 3, 3' 5, 5'-tetramethylbenzidine (TMB) were added and incubated for 15 minutes. The reaction was terminated by adding 50 μl of a stop solution (2 N H_2SO_4) to each well. Plates were read in a SpectroMax iD3 microplate reader (Molecular Devices, San Jose, CA, USA) at 450 nm.

2.7. Statistical Analysis

GraphPad Prism Software Version 8.4.0 (GraphPad Software Inc., San Diego, CA, USA) was used for statistical analysis. For experiments involving 2 groups, paired nonparametric *t*-tests (two-tailed) were performed. For experiments involving 3 or more groups, data were evaluated using two-way ANOVA with multiple comparison tests. Unless otherwise stated, data are expressed as mean ± SEM. The number of animals or measurements in each group is indicated in the figure legends. The significance level was set at $p<0.05$ for all comparisons. IHC Images were compared using Image J to quantify the stained areas. Cells quantified in the immune-stained liver section images were presented as the percentage of $F4/80^+$ (or $CD4^+$, $CD8^+$) cells per field (10× objective). For all analyses, we quantified 6 randomly chosen fields per section per mouse. The same threshold settings were used for all analyses.

3. Results

3.1. RNase L deficency alleviated NAFLD in mice fed with HFHCD

To determine the effect of RNase L on the development of NAFLD, RNase L WT and KO mice were fed with HFHCD for 12 and 22 weeks (designated as 12w and 22w). We performed H&E staining of the liver tissue sections to characterize the histopathological changes (Figure 1). For the 12w-HFHCD group, both types of mice developed to NASH as evidenced by increased oil droplets in the livers. However, the outcomes in WT mice were obviously more severe. Liver tissues from WT mice showed significant widespread macro-vesicular steatosis, hepatocyte ballooning degeneration, and portal and intralobular inflammation. By contrast, in RNase L KO mice, steatosis is most intense around the periportal areas, and portal inflammation was clearly mild. For the 22w-HFHCD group, the degree of steatosis seemed to decrease because of less fatty droplets observed, but inflammation was widely spread in both RNase L WT and KO mice as reflected by infiltrated immune cells as indicated with arrows. Overtly, more infiltrates were present in RNase L WT mice than that in KO mice.

To determine the identity of these infiltrated immune cells, immunohistochemistry (IHC) staining for macrophage/KCs maker F4/80 (Figure 2A) and T lymphocyte subtypes $CD4^+$ and $CD8^+$ (Figure 2B and 2C) were performed on the liver sections from the mice. Our data showed that the numbers of $F4/80^+$ macrophage/KCs, $CD4^+$ T cells (T helper cells) and $CD8^+$ T cells (cytotoxic T cells) were decreased in the livers of RNase L KO mice in compared to WT mice in both 12w- and 22w-HFHCD groups. Relative quantification by using the image J software indicated that F4/80 positive cells were 13.7% and 13.9% in RNase L WT mice compared to 7.23% and 7.1% in RNase L KO mice after fed with HFHCD for 12 and 22 weeks (Figure 2D). Specifically, livers from RNase L WT mice showed more hepatic crown-like structures (hCLS), clusters of macrophages aggregated around the remnant lipid droplets of steatotic dead/dying hepatocytes including cholesterol crystals [26], which is a prominent histological feature of NASH [27]. Portal inflammation is strongly associated with progressed NASH [28]. The populations of $CD4^+$ and $CD8^+$ cells were significantly higher, which are 6.5% and 2.85%, in the livers of RNase L WT mice compared to 1.72% and 0.65% in RNase L KO mice with HFHCF for 12 weeks. Interestingly, the populations of $CD4^+$ and $CD8^+$ cells were dramatically down in both types of mice fed with HFHCD for 22 weeks (Figure 2D), in which $CD4^+$ and $CD8^+$ T-cells were 0.72% and 1.15% in RNase L WT mice compared to 0.35% and 0.59% in RNase L KO mice. Overtly, T-cell associated immune responses mainly occurs in the early stage of NAFLD. Taken together, our results demonstrated that $CD4^+$ seemed to be the relative dominant cell types compared to $CD8^+$ T cells in portal inflammatory infiltrates during NASH. These findings suggest an important role of RNase L in mediating immune cell recruitment and liver inflammation in NAFLD.

The trichrome staining of the liver tissue section is commonly used to determine fibrosis and the stage of the disorder. It helps in identifying morphological alternations in the collagenous tissue of liver cirrhosis [29]. As shown in Figure 3, both RNase L WT and KO mice fed with HFHCD for 12 weeks showed a certain degree of periportal fibrosis, although the fibrotic status was slightly severe in the liver of RNase L WT mice than that in KO mice. After fed with HFHCD for 22 weeks, periportal and perisinusoidal fibrosis was more evident in both RNase L WT and KO mice. Clearly, more profound perisinusoidal fibrosis was observed in RNase L WT mice, implicating that RNase L plays a role in promoting fibrosis.

3.2. RNase L KO mice fed with HFHCD gained more body weight

Impaired lipid metabolism is one of the causes in development of NAFLD and studies have revealed that obesity is closely associated with an increased risk of fibrosis progression. To determine if RNase L is involved in lipid metabolism, we determined the body weight (BW) changes for both types of mice under HFHCD and the liver weight at the endpoint of the experiments. RNase L deficient mice gained more body weight than WT mice (Figure 4). However, there were no significant differences in the liver/BW ratios between WT and RL-KO mice, though WT slightly had higher liver/BW ratios at the endpoint. The complete statistical data of BW changes and the liver/BW ratios of mice are shown in Table 1. Bothe types of male mice (9-months-old) were fed with HFHCD for 22 weeks. At the end point, RNase L KO mice gained around 16.83 grams of BW which was equivalent to an increase

of 50.13% of their original BW compared to that WT mice gained around 11.86 grams of BW, which was equivalent to an increase of 28.94% of their original BW. To further confirm the result, we used a little older mouse to repeat the experiment. Bothe types of male mice (11-months-old) were fed with HFHCD for 12 weeks, RNase L KO mice gained around 10.38 grams of BW, which was equivalent to an increase of 23.75% of their original BW, while WT mice gained around 6.00 grams of BW, which was equivalent to an increase of 12.52% of their original BW. The data show that RNase L contributes to lipid metabolism and KO mice gain BW much faster, which is consistent with our previous observation [25].

3.3. RNase L deficiency altered liver biochemistry parameters

The liver biochemistry parameters in the blood are commonly evaluated clinically, which can be used to assess the liver functions. In this study, plasma glucose, total cholesterol, triglyceride, alanine transaminase (ALT), and aspartate transaminase (AST) were measured with a Veterinary Chemistry Analyzer (Table 2). Although glucose and total cholesterol levels in both types of mice from the 12w-HFHCD group remarkably increased, the level of total cholesterol was significantly higher in RNase L KO mice compared to that in WT mice (Figure 5 and Table 2). The levels of triglyceride in both types of mice were within the normal range. Interestingly, the levels of ALT and AST, two major enzymes clinically used to assess the function of the liver, in RNase L WT mice were significantly higher than in RNase L KO mice, indicating that hepatocyte damage was more severe in RNase L WT mice. However, in the 22w-HFHCD group, the levels of glucose and total cholesterol also increased in both genotypes of mice, though no significant difference was observed. Surprisingly, the levels of triglycerides were markedly reduced, possibly due to impairment in very low-density lipoprotein secretion from the livers [30]. Furthermore, the levels of ALT and AST in both types of mice were decreased, which might be associated with decreased hepatic steatosis and inflammation, and increased fibrosis. All suggest a broad and severe hepatocyte damage causes the loss of liver function and RNase L promotes the event.

3.4. RNase L deficiency affected complete blood count parameters

Complete blood count (CBC) is a blood test used to evaluate overall body health and detect a wide range of disorders. Studies have demonstrated that hematological parameters can provide useful information for monitoring NAFLD progression [31,32]. As shown in Table 3, the total WBC counts in both RNase L WT and KO mice in the 12w-HFHCD group were elevated beyond the upper limit of the normal range. Though the monocyte counts in both types of mice fell in the normal range, the population of monocytes in the blood of RNase L WT mice was remarkably higher than that in RNase L KO mice. Interestingly, RNase L WT mice fed with HFHCD for 22 weeks had almost the same counts of monocytes, but there was a significant difference in the population of total WBC, in particular lymphocytes. The total white blood cells (WBC) and lymphocytes were 56% and 43% higher in RNase L WT mice than that in KO mice. Most surprisingly, the counts of platelet in RNase L KO mice in the 12w-HFHCD group were 21.2% higher than that in RNase L WT mice. However, the population of platelets in RNase L WT mice was 62.8% higher than that in RNase L KO mice, a complete opposite manifestation, after those mice were fed with HFHCD for 22 weeks. The cause and biological significance need to be further investigated.

3.5. RNase L regulated the expression of certain cytokines and chemokines

It has been well established that inflammation promotes the development of NAFLD. Cytokines and chemokines play a pivotal role in inflammatory responses. To determine the effect of RNase L on the expression of cytokines and growth factors in the development of NAFLD, we measured the plasma levels of some critical cytokines or chemokines involved in inflammation and fibrosis in both RNase L WT and KO mice after fed with HFHCD. As shown in Figure 6, the levels of pro-inflammatory cytokines IL-1β, and chemokines CCL2, were substantially higher in WT mice compared to that in RNase L KO mice in the 12w-HFHCD group. In particular, the level of CCL2 remained 4-fold higher in the plasma of RNase L WT mice than that in RNase L KO mice although its levels were remarkably increased in both type of mice after fed with HFHCD for 22 weeks, indicating that the excessive expression of CCL2 regulated by RNase L may be one of the target molecules contributing to the severity of HFHCD-induced fibrogenesis. Furthermore, the levels of TGF-β, a fibrogenic factor, were remarkably increased but significantly higher in RNase L WT mice than that in RNase L KO mice. Interestingly, significantly higher levels of anti-inflammatory IL-10 were also observed in RNase L WT mice, though the physiological role of the enhanced IL-10 production in the lipid-induced hepatic fibrosis is largely unknown.

3.6. RNase L regulated the expression of some key genes in lipid metabolism, inflammation, and fibrotic signaling

Several signal pathways and effectors are believed to be involved in liver fibrogenesis. To determine if RNase L affects the pathogenesis of liver fibrosis, we analyzed the expression of some key genes in lipid metabolism, inflammation, and the activation of the signaling pathways associated with fibrosis. Liver tissue extracts prepared from RNase L WT and KO mice after fed with HFHCD for 12 and 22 weeks were subjected to immune blot analyses with antibodies against the selected target molecules. As shown in Figure 7, the expression of HMGCR, NLRP3, Caspase-1, Notch2 and MMP9 were markedly upregulated in RNase L WT mice of both 12w- and 22w-HFHCD groups. Moreover, the expression of Col1a1 was significantly higher expressed in the livers of RNase L WT mice in the 22w-HFHCD group, implicating the overproduction of collagen occurred, which may explain the severe status of fibrosis.

4. Discussion

NAFLD is excessive fat build-up in the liver without another clear cause such as alcohol use. It can progress to NASH, which may eventually lead to complications such as cirrhosis, liver cancer and liver failure, recognized as a major cause of the end-stage liver disease [33]. However, the molecular mechanism underlying the progression from simple steatosis to NASH is not well elucidated. Disrupted lipid homeostasis is a major cause of NAFLD. Several NAFLD models based on varying dietary manipulations have been developed [34]. The most popular one is to use a high cholesterol diet to induce a pronounced NASH phenotype in animal models [35-37]. In this study, we fed RNase L WT and KO mice with a high-fat diet containing 2% cholesterol for 12 and 22 weeks. The pathophysiological alternations and the development of NAFLD were monitored and analyzed in these mice.

The histological results showed that RNase L WT mice exhibited significantly more severe NASH, evidenced by widespread macro-vesicular steatosis, hepatocyte ballooning degeneration, inflammatory infiltrates, and fibrosis, suggesting that RNase L may be a potential target for lipid induced NAFLD progression and treatment of this disorder.

RNase L KO mice gained more body weight with about a 20% higher total cholesterol level than that in WT mice after fed with HFHCD for 12 weeks. However, there was no significant difference in the total cholesterol level between the two types of mice fed with HFHCD for 22 weeks. Surprisingly, the expression of HMGCR was dramatically higher in the livers of RNase L WT mice than that in RNase L KO mice although the cholesterol level in the plasma of RNase L KO mice was slightly higher after fed with HFHCD for 12 weeks. However, the physiological significance of the observation was largely unknown. It implicates that RNase L may be involved in suppressing the HMGCR degradation in the feedback regulation of cholesterol synthesis [38]. Interestingly, the levels of ALT and AST were remarkably increased in the mice fed with HFHCD, but they were significantly higher in RNase L WT mice than that in RNase L KO mice. The release of ALT and AST reflects the hepatic damage and inflammation, clinically used as one of the golden standards for assessing the function of the liver and indicating liver disease. The results suggest that feeding with HFHCD is able to induce liver damage and presence of RNase L can severe the event.

Inflammation in the absence of infection is as an important risk factor leading to liver injury in various acute and chronic liver disorders. During the pathogenesis of NAFLD, the activation of the NLRP3 inflammasome plays a vital role in the progression to NASH and cirrhosis [39]. The NLRP3 inflammasome activation promotes a wide range of immune responses including increased expression of proinflammatory cytokines and chemokines with the subsequent recruitment of immune cells and induction of cell death. Furthermore, studying the molecular mechanism underlying the contribution of NLRP3 to the progress of NASH reveals that assembly of NLRP3 with pro-Caspase-1 leads to cleavage of the latter into its active form, resulting in activation of some proinfmmatory cytokines such as IL-1β and triggering apoptosis [40]. It has been reported that viral infection-activated NLRP3 involves the 2-5A synthetase (OAS)/RNase L system, a component of the IFN-induced antiviral response that senses double-stranded RNA and activates RNase L to cleave viral and cellular RNAs. Interestingly, the levels of NLRP3 and caspase-1 were significantly higher in the livers of RNase L WT mice than that in RNase L KO mice after fed with HFHCD. Furthermore, the remarkable higher level of IL-1β in the plasma of RNase L WT mice was consistent with the outcome [19,41]. CCL2 is associated with monocyte/macrophage infiltration in the livers of patients with NASH and murine models of steatohepatitis and fibrosis [42,43]. Previously, we have reported that RNase L is necessary for CCL2 production in macrophages upon induction with LPS [21]. In this study, the levels of CCL2 in the plasma of RNase L WT mice after fed with HFHCD for 12 and 22 weeks were 4 and 2.4-fold higher than that in RNase L KO mice under the same condition. IL-10 displays the anti-fibrogenesis role in multiple organs including liver. However, the level of IL-10 was significantly higher in the plasma of RNase L WT mice fed with HFHCD. The role of IL-10 in this circumstance is largely unknown, which warrants further investigation. Taken together, our results suggest that RNase L contributes to the progressing of NASH, at

least in part, through upgradation of the NLRP3 inflammasome and other proinflammatory cytokines and chemokines, promoting inflammation in the liver.

NAFLD is a complex heterogeneous disease in which the histological features result from multiple nutritional and environmental exposures on a susceptible genetic background [44]. The observation that RNase L KO mice were more prone to accumulate fat than RNase L WT mice after fed with HFHCD seemed contradictory with the histological findings that WT mice developed more severe NASH. However, the correlation between weight gain and pathological phenotype in RNase L WT and KO mice fed with a high cholesterol diet is also unclear. Studies using different concentrations of a cholesterol diet show that mice fed a high-fat diet supplemented with 2% cholesterol have increased inflammation and fibrosis in the liver, while obesity, insulin resistance, and glucose intolerance are less pronounced compared to mice fed a chew diet [45]. Consistently, mice fed obesogenic diets with higher cholesterol levels, such as 1.5% and 2%, exhibited similar impairments in the liver [46,47]. It has well demonstrated that multiple factors and various signaling pathways such as TGF-1β, Col1a1, MMP9 and Notch2 are involved in the development of NAFLD, particularly progressing to NASH and fibrosis [48-52]. Our data show that TGF-1β is significantly higher in the plasma of RNase L WT mice than that in RNase L KO mice fed with HFHCD for 22 weeks. Furthermore, the expression of Col1a1, MMP9 and Notch2 in the livers of RNase L WT mice fed with HFHCD was markedly upregulated in compared to that in RNase L KO mice. All together suggest that RNase L, one of the key enzymes in the IFN functions against viral infection and cell proliferation, may play a pleiotropic role in the pathogenesis of NAFLD caused by abnormal nutrition and environment.

In summary, understanding the progression of NAFLD from simple hepatic steatosis to NASH has important physiological and clinical implications. Here we show evidence that RNase L may contribute to the progression of NASH by mediating metabolic activity, immune response, and tissue remodeling after liver injury. In contrast to the current dogma that RNase L mainly functions as a ribonuclease in the IFN action against viral infection, the results from the present study have advanced our knowledge about its diverse biological functions in human diseases. Currently, neither an efficient, accurate method can be used to evaluate and ensure a timely trial-inclusion, lifestyle prevention, and complications surveillance for these high-risk patients, nor pharmacological intervention therapy has been developed to treat NASH or related complications. Thus, our findings suggest that RNase L may be a novel target for NAFLD. Undoubtedly, more studies on the function of RNase L in the pathogenesis of NASH would provide promising solutions to the current problems.

Acknowledgement:

The authors thank Dr. Aaron F. Severson for critical reading and helpful comments on the manuscript.

Funding:

This work was supported by a grant from the National Institutes of Health (R15 HL145588-01) to A.Z and partially by the Center for Gene Regulation in Health and Disease and the Faculty Research Development Award, Cleveland State University. Abigail Ansah-Zame was supported by the T32 Training Grant of the National Institutes of Health (1T32HL150389-01A1).

Data Availability Statement

Data sharing is not applicable to this article as no big datasets were generated or analyzed during the current study. All biological results will be shared by the publication in the scientific community.

Abbreviations:

NAFLD	Nonalcoholic fatty liver disease
NASH	nonalcoholic steatohepatitis
HFHCD	high fat and high cholesterol diet
NLRP3	NLR family pyrin domain containing 3
WT	Wild type
KO	knockout
BW	body weight
HMGCR	3-hydroxy-3-methyl-glutaryl-coenzyme A reductase
IFN	interferon
ALT	alanine transaminase
AST	aspartate transaminase

References

1. Chalasani N, Younossi Z, Lavine JE, Charlton M, Cusi K, Rinella M, Harrison SA, Brunt EM; Sanyal AJ. The diagnosis and management of nonalcoholic fatty liver disease: Practice guidance from the American Association for the Study of Liver Diseases. Hepatology 2018; 67:328–357. [PubMed: 28714183]
2. Younossi Z, Tacke F, Arrese M, Chander Sharma B, Mostafa I, Bugianesi E, Wai-Sun Wong V, Yilmaz Y, George J, Fan J., et al. Global Perspectives on Nonalcoholic Fatty Liver Disease and Nonalcoholic Steatohepatitis. Hepatology 2019; 69:2672–2682. [PubMed: 30179269]
3. Loomba R, Friedman SL, Shulman GI. Mechanisms and disease consequences of nonalcoholic fatty liver disease. Cell. 2021; 184:2537–2564. [PubMed: 33989548]
4. Huang DQ, El-Serag HB, Loomba R. Global epidemiology of NAFLD-related HCC: trends, predictions, risk factors and prevention. Nat Rev Gastroenterol Hepatol 2021; 18:223–238. [PubMed: 33349658]
5. Noureddin M, Vipani A, Bresee C, Todo T, Kim IK, Alkhouri N, Setiawan VW, Tran T, Ayoub WS, Lu SC, et al. NASH Leading Cause of Liver Transplant in Women: Updated Analysis of Indications For Liver Transplant and Ethnic and Gender Variances. Am J Gastroenterol 2018; 113:1649–1659. [PubMed: 29880964]
6. Sheka AC, Adeyi O, Thompson J, Hameed B, Crawford PA, Ikramuddin S. Nonalcoholic Steatohepatitis: A Review. JAMA 2020; 323:1175–1183. [PubMed: 32207804]
7. Kazankov K, Jørgensen SMD, Thomsen KL, Møller HJ, Vilstrup H, George J, Schuppan D, Grønbæk H. The role of macrophages in nonalcoholic fatty liver disease and nonalcoholic steatohepatitis. Nature Reviews Gastroenterology & Hepatology 2019; 16:145–159. [PubMed: 30482910]

8. Peterson KR, Cottam MA, Kennedy AJ, Hasty AH. Macrophage-Targeted Therapeutics for Metabolic Disease. Trends Pharmacol Sci 2018; 39:536–546. [PubMed: 29628274]
9. Neuschwander-Tetri BA. Hepatic lipotoxicity and the pathogenesis of nonalcoholic steatohepatitis: the central role of nontriglyceride fatty acid metabolites. Hepatology 2010; 52: 774–788. [PubMed: 20683968]
10. Marra F, Svegliati-Baroni G. Lipotoxicity and the gut-liver axis in NASH pathogenesis. J Hepatol 2018; 68:280–295. [PubMed: 29154964]
11. Ioannou GN, Subramanian S, Chait A, Haigh WG, Yeh MM, Farrell GC, Lee SP, Savard C. Cholesterol crystallization within hepatocyte lipid droplets and its role in murine NASH. J Lipid Res 2017; 58:1067–1079. [PubMed: 28404639]
12. Savard C, Tartaglione EV, Kuver R, Haigh WG, Farrell GC, Subramanian S, Chait A, Yeh MM, Quinn LS, Ioannou GN. Synergistic interaction of dietary cholesterol and dietary fat in inducing experimental steatohepatitis. Hepatology 2013; 57:81–92. [PubMed: 22508243]
13. Kunjathoor VV, Febbraio M, Podrez EA, Moore KJ, Andersson L, Koehn S, Rhee JS, Silverstein R, Hoff HF, Freeman MW. Scavenger receptors class A-I/II and CD36 are the principal receptors responsible for the uptake of modified low density lipoprotein leading to lipid loading in macrophages. J Biol Chem 2002; 277:49982–49988. [PubMed: 12376530]
14. Wree A, Eguchi A, McGeough MD, Pena CA, Johnson CD, Canbay A, Hoffman HM, Feldstein AE. NLRP3 inflammasome activation results in hepatocyte pyroptosis, liver inflammation, and fibrosis in mice. Hepatology 2014; 59:898–910. [PubMed: 23813842]
15. Zhou A, Hassel BA, Silverman RH. Expression cloning of 2-5A-dependent RNAase: a uniquely regulated mediator of interferon action. Cell 1993; 72:753–765. [PubMed: 7680958]
16. Silverman RH. Viral encounters with 2',5'-oligoadenylate synthetase and RNase L during the interferon antiviral response. J Virol 2007; 81:12720–12729. [PubMed: 17804500]
17. Zhou A, Paranjape J, Brown TL, Nie H, Naik S, Dong B, Chang A, Trapp B, Fairchild R, Colmenares C, et al. Interferon action and apoptosis are defective in mice devoid of 2',5'-oligoadenylate-dependent RNase L. Embo j 1997; 16:6355–6363. [PubMed: 9351818]
18. Malathi K, Dong B, Gale M Jr, Silverman RH. Small self-RNA generated by RNase L amplifies antiviral innate immunity. Nature 2007; 448:816–819. [PubMed: 17653195]
19. Chakrabarti A, Banerjee S, Franchi L, Loo YM, Gale M Jr, Núñez, G, Silverman RH. RNase L activates the NLRP3 inflammasome during viral infections. Cell Host Microbe 2015; 17:466–477. [PubMed: 25816776]
20. Zeng C, Yi X, Zipris D, Liu H, Zhang L, Zheng Q, Malathi K, Jin G, Zhou A. RNase L contributes to experimentally induced type 1 diabetes onset in mice. J Endocrinol 2014; 223: 277–287. [PubMed: 25287058]
21. Yi X, Zeng C, Liu H, Chen X, Zhang P, Yun BS, Jin G, Zhou A. Lack of RNase L attenuates macrophage functions. PLoS One 2013; 8: e81269. [PubMed: 24324683]
22. Wei R, Chen G, Algehainy N, Zeng C, Liu C, Liu H, Liu W, Stacey D, Zhou A. RNase L Is Involved in Liposaccharide-Induced Lung Inflammation. Viruses 2020; 12, doi:10.3390/v12010073.
23. Yin H, Jiang Z, Wang S, Zhang P. IFN-γ restores the impaired function of RNase L and induces mitochondria-mediated apoptosis in lung cancer. Cell Death Dis 2019; 10:642. [PubMed: 31501431]
24. Ma Q, Li J, Zhou H, Tong W, Chen Y. The function of RNase L and its degradation mechanism in cardiac acute ischemic injury. Apoptosis 2020; 25:400–411. [PubMed: 32385693]
25. Fabre O, Salehzada T, Lambert K, Boo Seok Y, Zhou A, Mercier J, Bisbal C. RNase L controls terminal adipocyte differentiation, lipids storage and insulin sensitivity via CHOP10 mRNA regulation. Cell Death Differ 2012; 19:1470–1481. [PubMed: 22441668]
26. Murano I, Barbatelli G, Parisani V, Latini C, Muzzonigro G, Castellucci M, Cinti S. Dead adipocytes, detected as crown-like structures, are prevalent in visceral fat depots of genetically obese mice. J Lipid Res 2008; 49:1562–1568. [PubMed: 18390487]
27. Ioannou GN, Haigh WG, Thorning D, Savard C. Hepatic cholesterol crystals and crown-like structures distinguish NASH from simple steatosis[S]. Journal of Lipid Research 2013; 54: 1326–1334. [PubMed: 23417738]

28. Gadd VL, Skoien R, Powell EE, Fagan KJ, Winterford C, Horsfall L, Irvine K, Clouston AD. The portal inflammatory infiltrate and ductular reaction in human nonalcoholic fatty liver disease. Hepatology 2014; 59:1393–1405. [PubMed: 24254368]
29. Levy JJ, Azizgolshani N, Andersen MJ Jr, Suriawinata A, Liu X, Lisovsky M, Ren B, Bobak CA, Christensen BC, Vaickus LJ. A large-scale internal validation study of unsupervised virtual trichrome staining technologies on nonalcoholic steatohepatitis liver biopsies. Mod Pathol 2021; 34:808–822. [PubMed: 33299110]
30. Hugh P, Barrett R. Kinetics of triglyceride rich lipoproteins: chylomicrons and very low density lipoproteins. Atherosclerosis 1998; 141 Suppl 1, S35–40. [PubMed: 9888640]
31. Michalak A, Guz M, Kozicka J, Cybulski M, Jeleniewicz W, Lach T, Cichoż-Lach H. Red blood cell distribution width derivatives in alcohol-related liver cirrhosis and metabolic-associated fatty liver disease. World J Gastroenterol 2022; 28:5636–5647. [PubMed: 36304090]
32. Tarantino G, Barrea L, Capone D, Citro V, Mosca T, Savastano S. Hematocrit Values Predict Carotid Intimal-Media Thickness in Obese Patients With Non-Alcoholic Fatty Liver Disease: A Cross-Sectional Study. Front Endocrinol (Lausanne) 2018; 9:203. [PubMed: 29760679]
33. Goldberg D, Ditah IC, Saeian K, Lalehzari M, Aronsohn A, Gorospe EC, Charlton M. Changes in the Prevalence of Hepatitis C Virus Infection, Nonalcoholic Steatohepatitis, and Alcoholic Liver Disease Among Patients With Cirrhosis or Liver Failure on the Waitlist for Liver Transplantation. Gastroenterology 2017; 152:1090–1099.e1091. [PubMed: 28088461]
34. Santhekadur PK, Kumar DP, Sanyal AJ. Preclinical models of non-alcoholic fatty liver disease. J Hepatol 2018; 68:230–237. [PubMed: 29128391]
35. Matsuzawa N, Takamura T, Kurita S, Misu H, Ota T, Ando H, Yokoyama M, Honda M, Zen Y, Nakanuma Y, et al. Lipid-induced oxidative stress causes steatohepatitis in mice fed an atherogenic diet. Hepatology 2007; 46:1392–1403. [PubMed: 17929294]
36. Liang JQ, Teoh N, Xu L, Pok S, Li X, Chu ESH, Chiu J, Dong L, Arfianti E, Haigh WG, et al. Dietary cholesterol promotes steatohepatitis related hepatocellular carcinoma through dysregulated metabolism and calcium signaling. Nat Commun 2018; 9:4490. [PubMed: 30367044]
37. McGettigan B, McMahan R, Orlicky D, Burchill M, Danhorn T, Francis P, Cheng LL, Golden-Mason L, Jakubzick CV, Rosen HR. Dietary Lipids Differentially Shape Nonalcoholic Steatohepatitis Progression and the Transcriptome of Kupffer Cells and Infiltrating Macrophages. Hepatology 2019; 70:67–83. [PubMed: 30516830]
38. Schumacher MM, DeBose-Boyd RA. Posttranslational Regulation of HMG CoA Reductase, the Rate-Limiting Enzyme in Synthesis of Cholesterol. Annu Rev Biochem 2021; 90:659–679. [PubMed: 34153214]
39. Knorr J, Wree A, Tacke F, Feldstein AE. The NLRP3 Inflammasome in Alcoholic and Nonalcoholic Steatohepatitis. Semin Liver Dis 2020; 40:298–306. [PubMed: 32526788]
40. Mridha AR, Wree A, Robertson AAB, Yeh MM, Johnson CD, Van Rooyen DM, Haczeyni F, Teoh NC, Savard C, Ioannou GN, et al. NLRP3 inflammasome blockade reduces liver inflammation and fibrosis in experimental NASH in mice. J Hepatol 2017; 66:1037–1046. [PubMed: 28167322]
41. Banerjee S. RNase L and the NLRP3-inflammasome: An old merchant in a new trade. Cytokine Growth Factor Rev 2016; 29:63–70. [PubMed: 26987611]
42. Weisberg SP, Hunter D, Huber R, Lemieux J, Slaymaker S, Vaddi K, Charo I, Leibel RL, Ferrante AW Jr. CCR2 modulates inflammatory and metabolic effects of high-fat feeding. J Clin Invest 2006;116:115–124. [PubMed: 16341265]
43. Baeck C, Wehr A, Karlmark KR, Heymann F, Vucur M, Gassler N, Huss S, Klussmann S, Eulberg D, Luedde T, et al. Pharmacological inhibition of the chemokine CCL2 (MCP-1) diminishes liver macrophage infiltration and steatohepatitis in chronic hepatic injury. Gut 2012; 61:416–426. [PubMed: 21813474]
44. Arrese M, Arab JP, Barrera F, Kaufmann B, Valenti L, Feldstein AE. Insights into Nonalcoholic Fatty-Liver Disease Heterogeneity. Semin Liver Dis 2021; 41:421–434. [PubMed: 34233370]
45. Zhang H, Léveillé M, Courty E, Gunes A, Estall JL. Differences in metabolic and liver pathobiology induced by two dietary mouse models of nonalcoholic fatty liver disease. Am J Physiol Endocrinol Metab 2020; 319:E863–e876. [PubMed: 32924526]

46. Komatsu G, Nonomura T, Sasaki M, Ishida Y, Arai S, Miyazaki T. AIM-deficient mouse fed a high-trans fat, high-cholesterol diet: a new animal model for nonalcoholic fatty liver disease. Exp Anim 2019; 68:147–158. [PubMed: 30487357]

47. Eng JM, Estall JL. Diet-Induced Models of Non-Alcoholic Fatty Liver Disease: Food for Thought on Sugar, Fat, and Cholesterol. Cells 2021; 10: doi:10.3390/cells10071805.

48. Schwabe RF, Tabas I, Pajvani UB. Mechanisms of Fibrosis Development in Nonalcoholic Steatohepatitis. Gastroenterology 2020;158:1913–1928. [PubMed: 32044315]

49. Schuppan D, Surabattula R, Wang XY. Determinants of fibrosis progression and regression in NASH. J Hepatol 2018; 68:238–250. [PubMed: 29154966]

50. Coilly A, Desterke C, Guettier C, Samuel D, Chiappini F. FABP4 and MMP9 levels identified as predictive factors for poor prognosis in patients with nonalcoholic fatty liver using data mining approaches and gene expression analysis. Sci Rep 2019; 9:19785. [PubMed: 31874999]

51. Zhu C, Kim K, Wang X, Bartolome A, Salomao M, Dongiovanni P, Meroni M, Graham MJ, Yates KP, Diehl AM, et al. Hepatocyte Notch activation induces liver fibrosis in nonalcoholic steatohepatitis. Sci Transl Med 2018; 10: doi:10.1126/scitranslmed.aat0344.

52. Yu J, Zhu C, Wang X, Kim K, Bartolome A, Dongiovanni P, Yates KP, Valenti L, Carrer M, Sadowski T, et al. Hepatocyte TLR4 triggers inter-hepatocyte Jagged1/Notch signaling to determine NASH-induced fibrosis. Sci Transl Med 2021; 13: doi:10.1126/scitranslmed.abe1692.

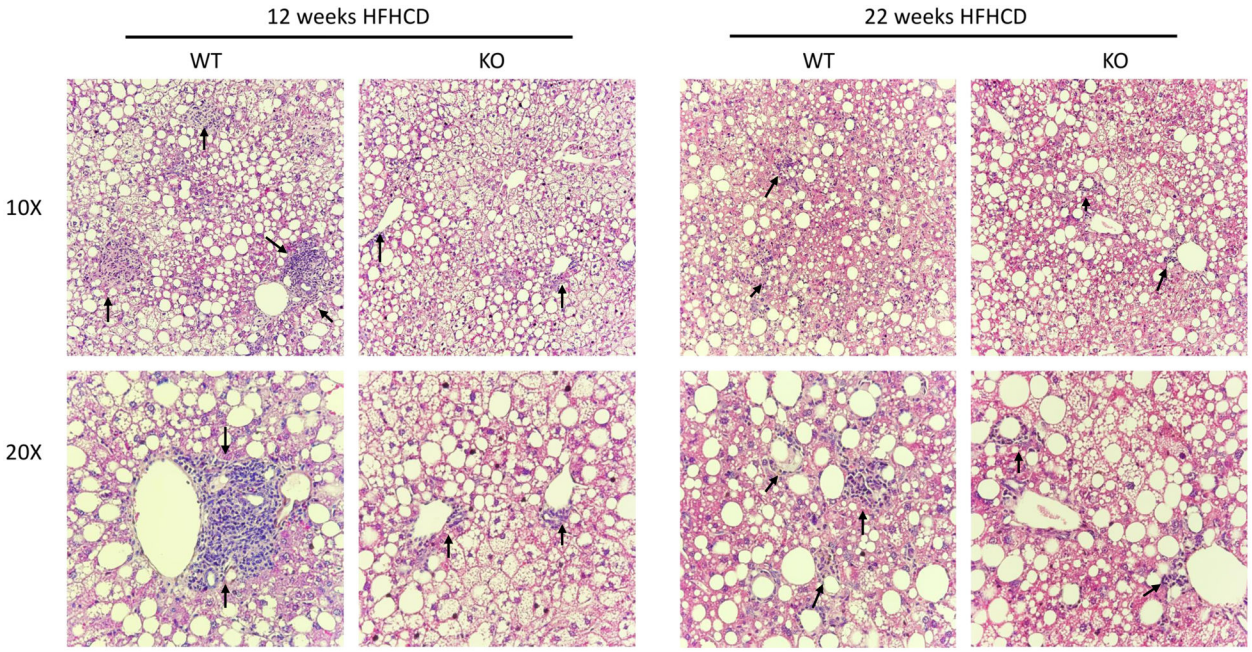

Figure 1. H&E staining of liver tissues from HFHCD-fed mice

Age-matched adult male RNase L WT and KO mice (n=8/group) were fed with HFHCD containing 2% cholesterol for either 12 or 22 weeks. Histological changes in the liver structures after fed with HFHCD are shown. Representative images of H&E stained sections of liver tissues are present at 10× and 20× magnifications. Black arrows indicate the infiltrated immune cells (blue).

A. F4/80⁺ Macrophages

IHC – F4/80

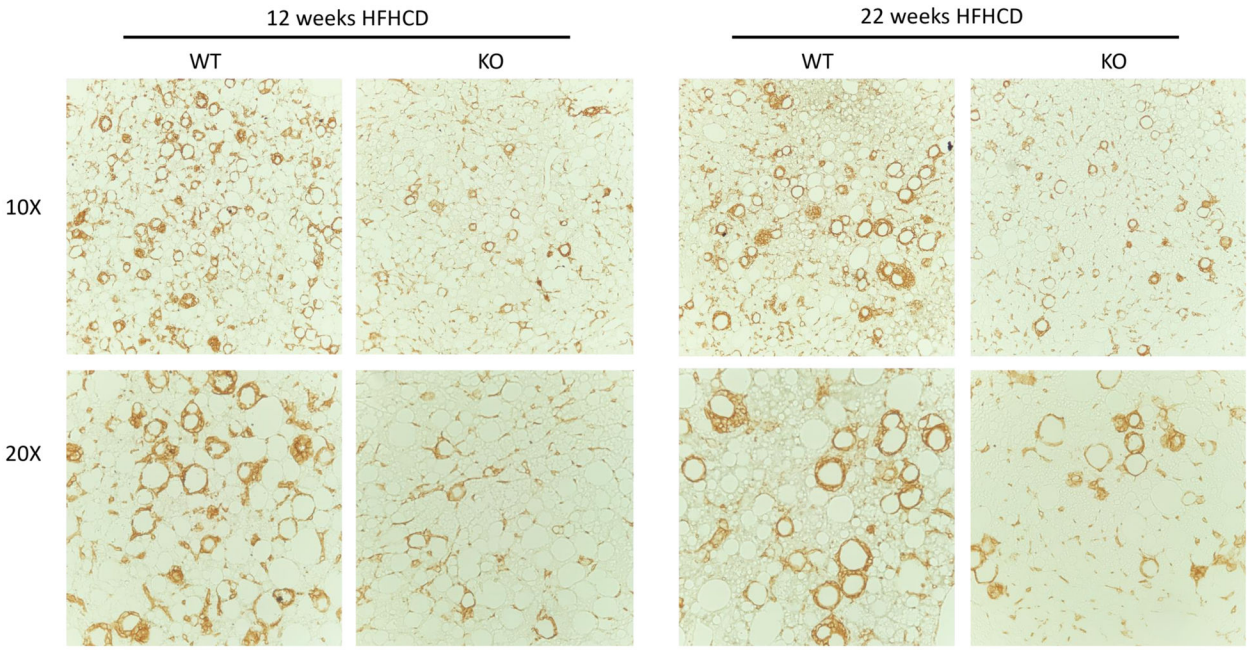

B. CD4⁺ T cells

IHC – CD4

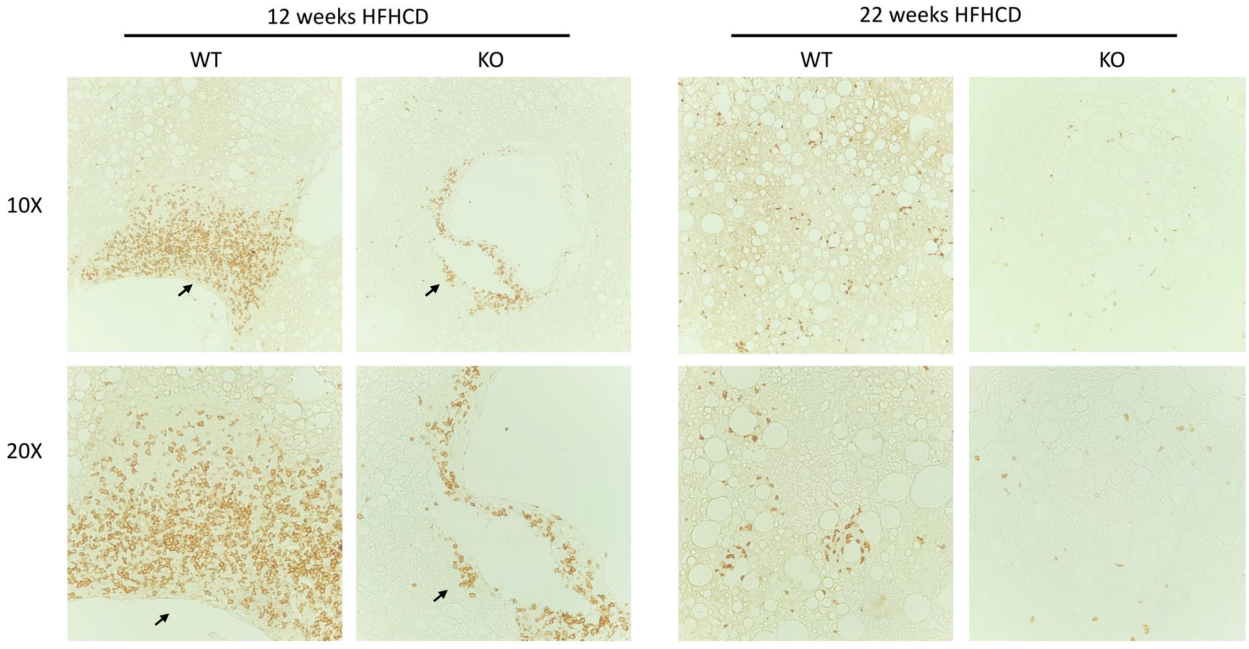

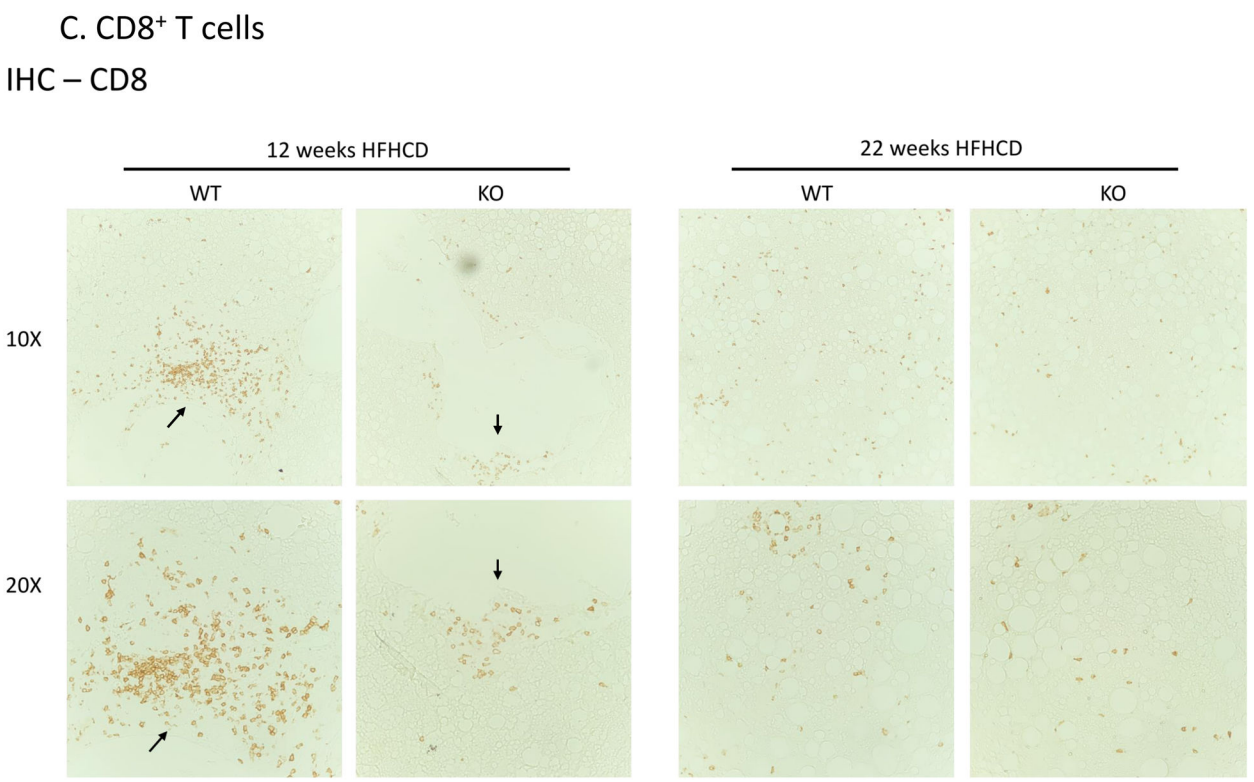

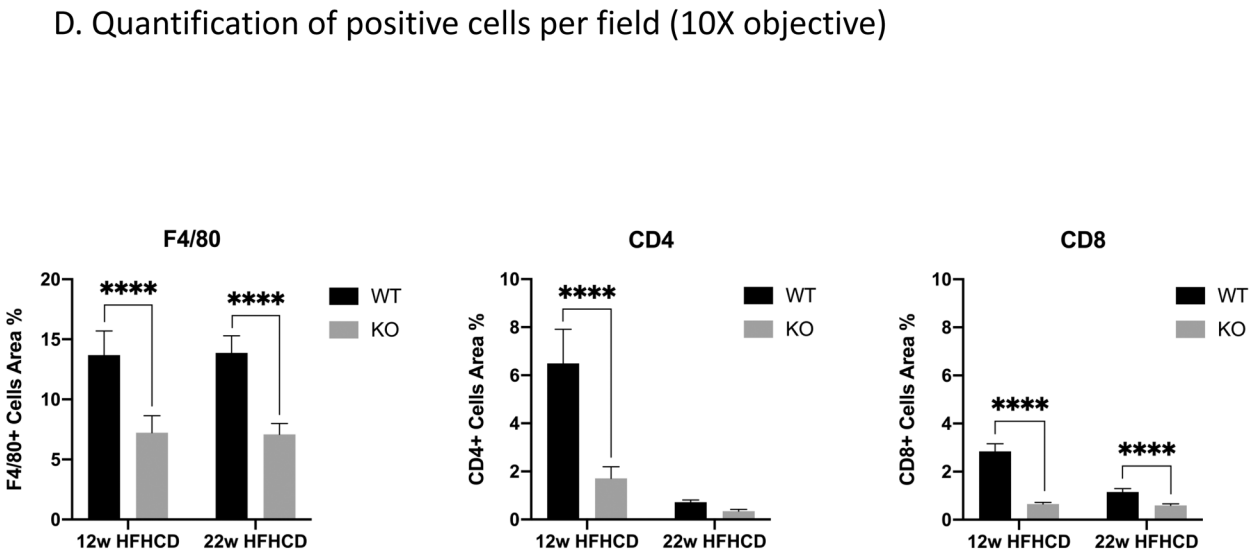

Figure 2. Infiltration of immune cells in the livers of mice fed with HFHCD

Immune cells were infiltrated into the livers of RNase L WT and KO mice fed with HFHCD containing 2% cholesterol for either 12 or 22 weeks. The cell types were identified by immunohistostaining with (A) F4/80, (B) CD4, and (C) CD8. Representative images are present at 10× and 20× magnifications. Black arrows indicate the infiltrated immune cells. (D) Quantification of positive cells per field (10X objective). Values are present as means ± SEM (****$p < 0.0001$).

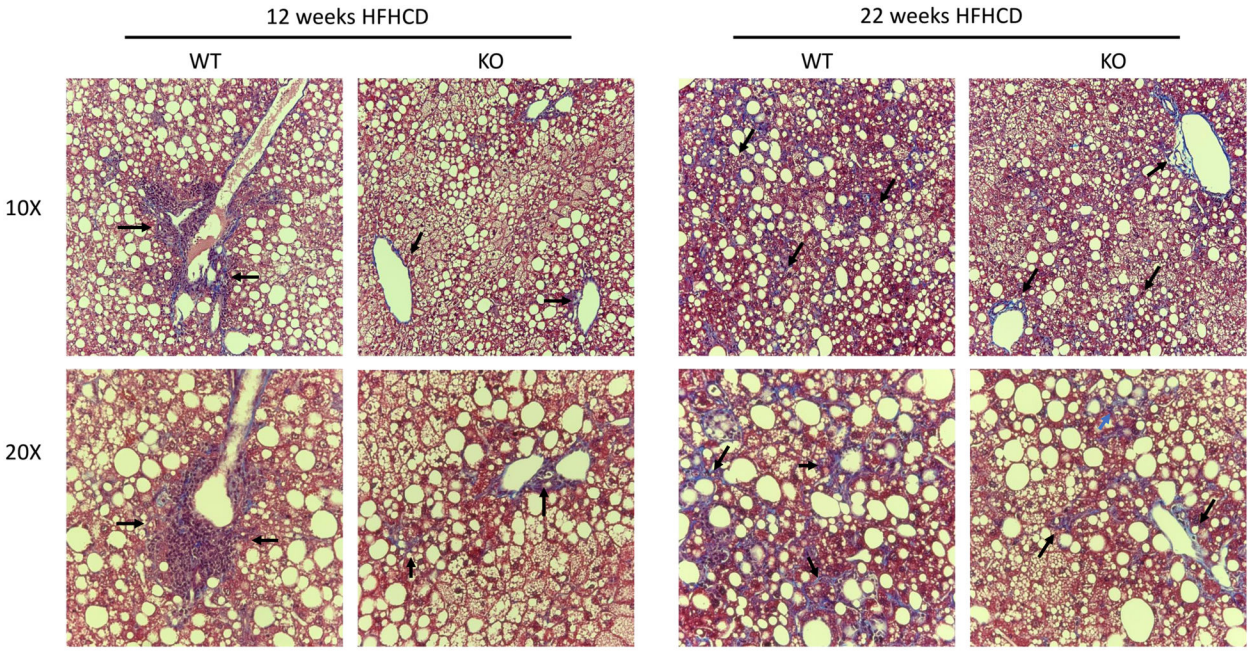

Figure 3. Trichrome staining of liver tissues from mice fed with HFHCD

Age-matched adult male RNase L WT and KO mice (n=8/group) were fed with HFHCD containing 2% cholesterol for either 12 or 22 weeks. The fibrotic status in the liver tissues after fed with HFHCD is shown (blue). Representative images of Trichrome staining processed sections of liver tissues are present at 10× and 20× magnifications.

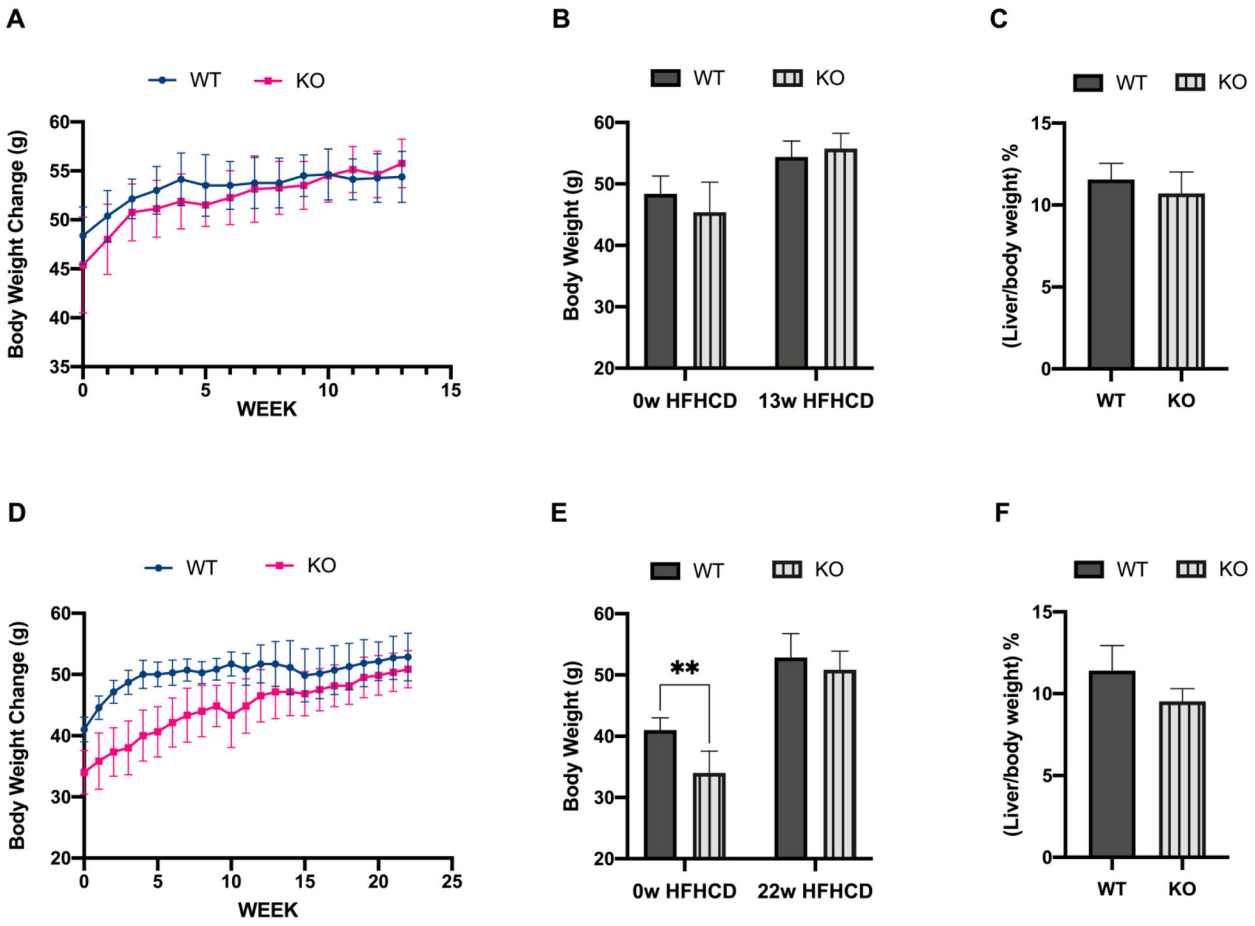

Figure 4. Bodyweight and liver/body weight ratio of mice fed with HFHCD

RNase L WT and KO mice (n= 8/group) were fed with HFHCD for either 12 (A-C) or 22 (D-F) weeks, and the mice were weighed every week; values are means ± SEM (*$p < 0.05$, **$p < 0.01$, ***$p < 0.001$).

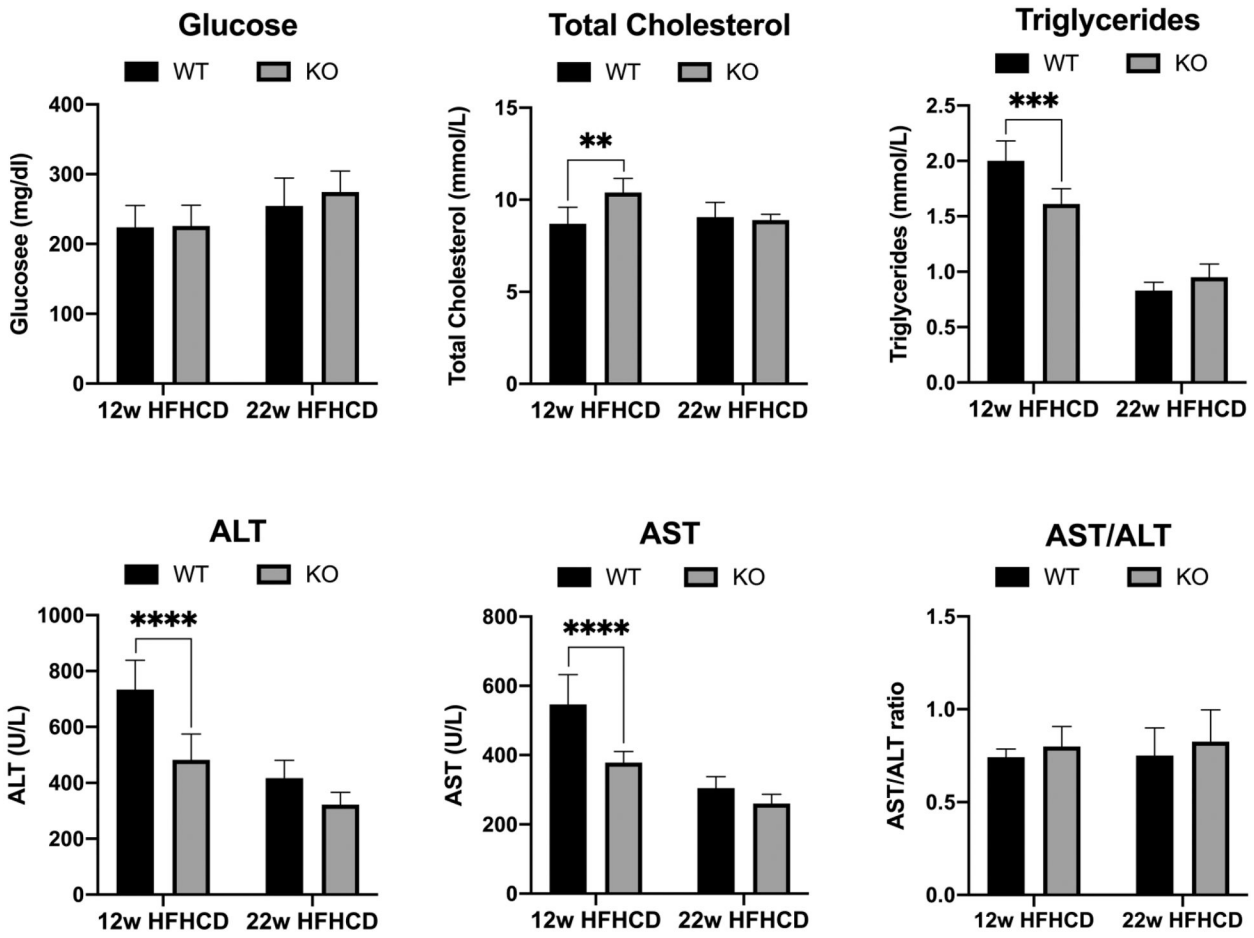

Figure 5. Liver biochemistry parameters of mice fed with HFHCD

RNase L WT and KO mice (n=6/group) were fed with HFHCD for either 12 or 22 weeks. Plasma biochemistry parameters for the liver function were analyzed by a veterinary chemistry analyzer; values are means ± SEM (*p < 0.05, **p < 0.01, ***p < 0.001, ****p < 0.0001).

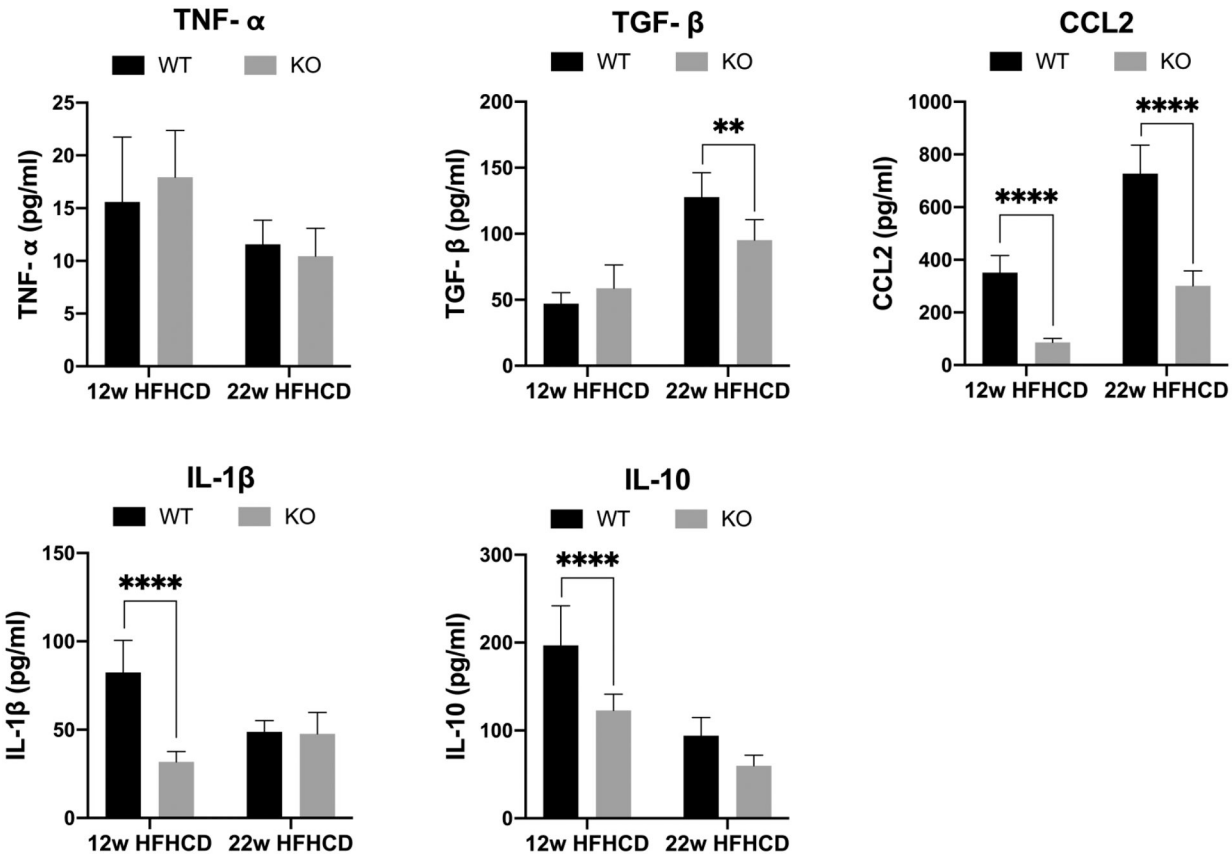

Figure 6. Levels of certain cytokines and chemokines in the plasma of mice fed with HFHCD

RNase L WT and KO mice (n=7-8/group) were fed with HFHCD for either 12 or 22 weeks. Cytokines in plasma were analyzed by ELISA; values are means ± SEM (*p < 0.05, **p < 0.01, ***p < 0.001, ****p < 0.0001).

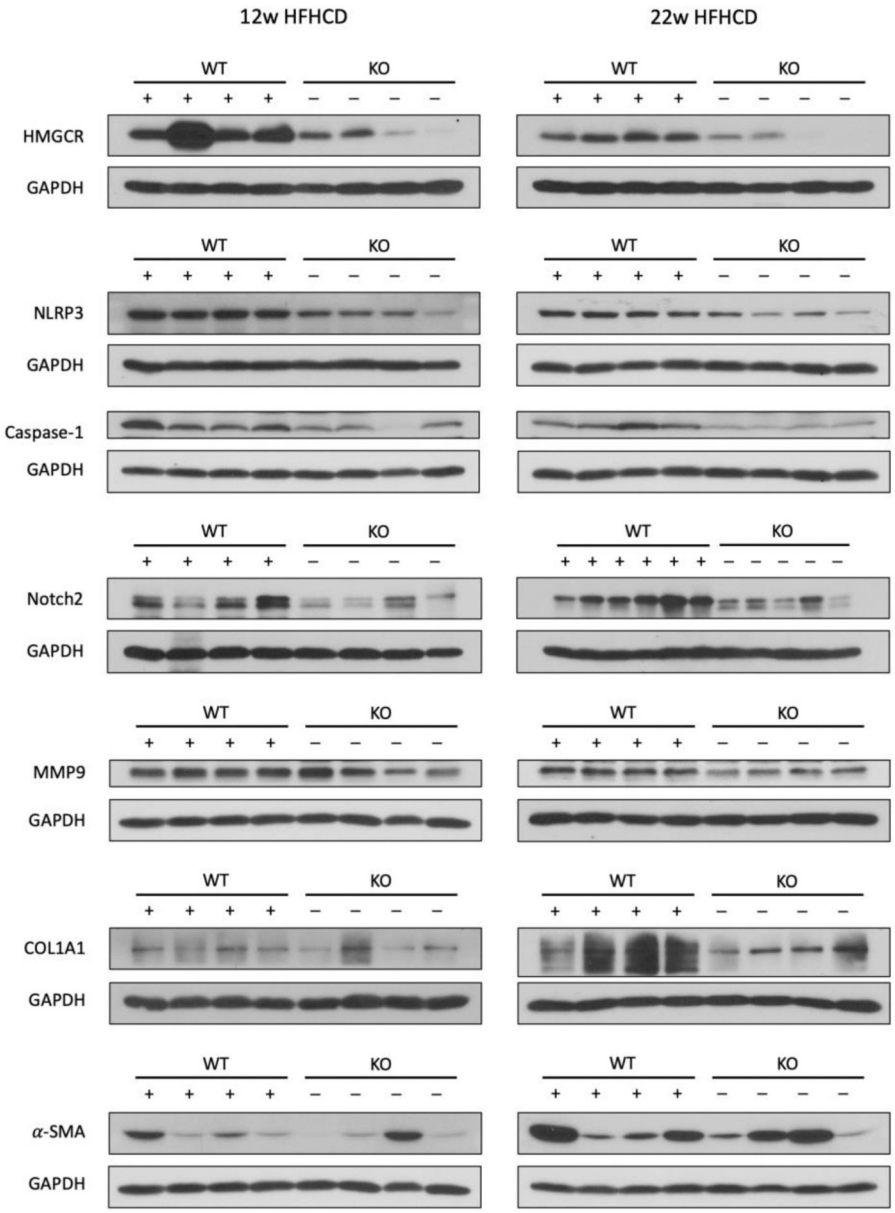

Figure 7. Expression of key genes involved in cholesterol metabolism, inflammation, and fibrosis pathways in the livers of mice fed with HFHCD.

Tissue extracts (100 mg protein/ each sample) prepared from the livers of RNase L WT and KO mice fed with HFHCD for either 12 or 22 weeks were analyzed by Western blot with antibodies against HMGCR, NLRP3, Caspase-1, Notch 2, α-SMA and COL1A1 (Cell Signaling); MMP9 (Abcam). GAPDH (Santa Cruz) was used for protein normalization. The same control was used for MMP9/α-SMA or NLRP3/Caspase-1in each of the experiments.

Table 1.

Statistical data of the body weight and liver/body weight ratios of mice fed with HFHCD

	12 weeks HFHCD			22 weeks HFHCD		
Variable	**WT**	**KO**	**P value**	**WT**	**KO**	**P value**
Initial BW (g)	48.38 ± 2.93	45.38 ± 4.90	0.0165	41.00 ± 2.00	34.00 ± 3.578	0.0014 **
Final BW (g)	54.38 ± 2.62	55.75 ± 2.50	0.6661	52.86 ± 3.89	50.83 ± 3.06	0.4646
Gained BW (g)	6.00 ± 1.51	10.38 ± 3.54	0.0015 **	11.86 ± 3.19	16.83 ± 0.75	0.0129 *
Gained BW/Initial BW (%)	12.52 ± 3.56	23.75 ± 20.23	0.0038 **	28.94 ± 7.86	50.13 ± 7.32	0.0089 **
Liver weight (g)	6.26 ± 0.62	5.97 ± 0.65	0.4243	6.08 ± 1.20	4.85 ± 0.58	0.0437 *
Liver/Final BW (%)	11.56 ± 0.99	10.71 ± 1.30	0.0897	11.41 ± 1.53	9.53 ± 0.78	0.1157

Table 2.

Statistical data of liver biochemistry parameters of mice fed with HFHCD

		12 weeks HFHCD			22 weeks HFHCD		
Plasma Variables	**Normal range**	**WT**	**KO**	**P value**	**WT**	**KO**	**P value**
Glucose	90-192 (mg/dl)	224 ± 31	226 ± 30	0.9921	254 ± 40	274 ± 30	0.5104
Total cholesterol	1.50-3.30 (mmol/L)	8.69 ± 0.90	10.39 ± 0.77	0.0013**	9.06 ± 0.80	8.89 ± 0.32	0.9049
Triglycerides	0.75-2.57 (mmol/L)	2.00 ± 0.18	1.61 ± 0.14	0.0001***	0.83 ± 0.08	0.95 ± 0.12	0.2539
ALT	18-94 (U/L)	734 ± 105	482 ± 93	<0.0001****	417 ± 64	322 ± 44	0.1048
AST	32-122 (U/L)	546 ± 87	387 ± 32	<0.0001****	305 ± 33	260 ± 27	0.2610
AST/ALT Ratio	N/A	0.74 ± 0.04	0.80 ± 0.11	0.6834	0.75 ± 0.15	0.82 ± 0.17	0.5381

Table 3.

Statistical data of complete blood count (CBC) parameters in mice fed with HFHCD

Variables	Normal range	Unit	12 weeks HFHCD			22 weeks HFHCD		
			WT	KO	P value	WT	KO	P value
WBC	0.80 - 10.60	10^3/uL	11.01 ± 1.81	11.05 ± 2.29	0.9734	10.98 ± 2.21	8.35 ± 0.49	0.0297 *
NEU	0.23 - 3.60	10^3/uL	2.68 ± 0.43	2.74 ± 0.47	0.8286	2.29 ± 0.61	2.02 ± 0.31	0.2482
LYM	0.60 - 8.90	10^3/uL	7.26 ± 1.68	7.56 ± 1.67	0.7551	7.61 ± 2.29	5.31 ± 0.91	0.0159 *
MONO	0.04 - 1.40	10^3/uL	0.82 ± 0.21	0.54 ± 0.16	0.0475 *	0.89 ± 0.26	0.87 ± 0.42	0.9561
EOS	0.00 - 0.51	10^3/uL	0.14 ± 0.11	0.13 ± 0.03	0.8759	0.13 ± 0.05	0.13 ± 0.03	0.7397
BAS	0.00 - 0.12	10^3/uL	0.11 ± 0.06	0.08 ± 0.02	0.4451	0.08 ± 0.03	0.04 ± 0.01	0.0278 *
NEU%	6.5 - 50.0	%	24.6 ± 3.9	25.0 ± 1.49	0.7966	20.9 ± 1.6	24.2 ± 3.5	0.0093 **
LYM%	40.0 - 92.0	%	65.5 ± 8.08	68.2 ± 1.4	0.4174	68.9 ± 3.5	63.2 ± 8.2	0.0584
MONO%	0.9 - 18.0	%	7.5 ± 1.4	4.8 ± 0.6	0.0074 **	8.3 ± 2.5	10.6 ± 5.3	0.2165
EOS%	0.0 - 7.5	%	1.3 ± 1.2	1.2 ± 0.4	0.9029	1.1 ± 0.4	1.5 ± 0.4	0.1242
BAS%	0.0 - 1.5	%	1.1 ± 0.8	0.8 ± 0.1	0.4092	0.7 ± 0.4	0.5 ± 0.1	0.1854
RBC	6.50 - 11.50	10^6/uL	8.82 ± 0.35	9.94 ± 0.08	0.0007 ***	9.69 ± 0.70	10.40 ± 0.58	0.2242
HGB	11.0 - 16.5	g/dL	13.6 ± 0.4	14.9 ± 0.1	0.0011 **	14.3 ± 0.8	14.6 ± 0.7	0.4850
HCT	35.0 - 55.0	%	44.0 ± 1.5	47.3 ± 0.5	0.0070 **	47.7 ± 3.1	48.9 ± 2.4	0.5595
MCV	41.0 - 55.0	fL	49.8 ± 1.3	47.6 ± 0.2	0.0121 *	49.2 ± 0.9	47.1 ± 0.6	0.0028 **
MCH	13.0 - 18.0	pg	15.5 ± 0.7	15.0 ± 0.1	0.1216	14.7 ± 0.4	14.1 ± 0.3	0.0363 *
MCHC	30.0 - 36.0	g/dL	31.1 ± 0.9	31.5 ± 0.4	0.2803	29.9 ± 0.5	29.9 ± 0.2	0.8260
RDW%	12.0 - 19.0	&	15.3 ± 0.9	14.6 ± 0.2	0.1361	14.5 ± 0.6	13.5 ± 0.3	0.0232 *
PLT	400 - 1600	10^3/uL	940 ± 121	1140 ± 86	0.0196 *	1449 ± 266	890 ± 188	0.0005 ***
MPV	4.0 - 6.2	fL	6.0 ± 0.3	5.6 ± 0.2	0.0519	5.8 ± 0.3	6.0 ± 0.2	0.1191